Journal of Himalayan Earth Sciences Volume 52, No. 1, 2019 pp. 37-50

Application of sub-pixel-based technique "orthorectification of optically sensed images and its correlation" for co-seismic landslide detection and its accuracy modification through the integration of various masks

Sumbal Bahar Saba, Nimat Ullah Khattak, Muhammad Ali, Muhammad Waseem, Samina Siddiqui, Seema Anjum, Syed Ali Turab

National Center of Excellence in Geology (NCEG), University of Peshawar, Pakistan,
**Corresponding authors email: sumbal_saba2000@yahoo.com*
Submitted:6/1/2019 Accepted:7/3/2019 Published online:29/3/2019

Abstract

Customary co-seismic landslide detection methods are meticulous, time demanding and very difficult to be adopted for regional-scale assessment. To provide on time fast and updated slope failure information, over the years numerous remote sensing based semi-automatic landslide detection methods have been developed and applied. However, implementation of these techniques requires some vital considerations like accurate and precise geometric correction, resampling and false positives elimination. To address these issues a new change-detection based technique of COSI-Corr (Co-registration of Optically Sensed Images and Correlation) has been adopted for mapping co-seismic landslides in Muzaffarabad area. However, due to COSI-Corr high sensitivity for detecting changes on the sub-pixel level, it is prone to detecting changes caused by vegetation, erosion and variation in built-up area size as false positive values. In this study, the influence of various factors like vegetation, sedimentation, erosion and built-up areas on landslides automatic detection results accuracy has been investigated. After the implementation of COSI-Corr technique, stepwise masking is performed. The false positives are successively removed from the landslide class by eliminating the noises resulting from drainage, urban sprawl and vegetation phonology. The results accuracy was increased after the application of each mask. The number of false positives was greatly reduced by the application of the vegetation-based mask. The best threshold found was 0.1 for which error of omission and error of commission was less than 11%. The results also showed that satellite images with medium spatial resolution could be successfully employed for the automatic detection of co-seismic landslides.

Keywords: COSI-Corr, Co-seismic landslides, False positives, Automatic technique.

1. Introduction

Customary co-seismic landslide detection methods are conscientious, time demanding and very difficult to be adopted for regional scale landslides assessment. To provide on time fast and updated slope failure information over the years numerous Remote Sensing (RS) based semi-automatic methods have been developed and applied. RS based techniques offer on time disaster responses over regional scale, especially for hard-hit and difficult-to-access areas (Vu et al., 2005). These techniques include pixel-based (Delacourt et al., 2004; Keyport et al., 2018; Moosavi et al., 2014; Sibaruddin et al., 2018), object-based (Aghighi et al., 2015; Barlow et al., 2006; Casagli et al., 2016; Ling et al., 2008; Martha et al., 2010; Martin and Franklin, 2005; N. Keyport et al., 2018) and sub-pixel based techniques (Mertens et al., 2008; Thornton et al., 2006).

The main problem in landslide identification while using RS based semi-automatic techniques is mainly limited by the spatial resolution of the sensor. Landslides, as compare to other geographic objects, are comparatively trivial in size. Therefore, most of the times changes in landslides or failing slopes appear to be on the sub-pixel level, making it tough for pixel-based and object-based techniques to be successfully detected (Delacourt et al., 2004; Yamaguchi et al., 2003). On the other hand, most of the landslide detection methods based on images comparison are frequently applied by using high-resolution imagery (Feizizadeh et al., 2017; Lee and Lee, 2006; Mondini et al., 2011; Nichol and Wong, 2005; Tsai et al., 2010; Weirich and Blesius, 2007). In this kind of analysis, high cost and pre-and post-event requirement of very high-resolution data (Mondini et al., 2011), makes it impossible to be adopted on a regional scale. Therefore, constant exertion is essential to

expand the mentioned techniques for effective landslide detection (Debella-Gilo and Kääb, 2011).

Implementation of RS based techniques require some vigorous considerations like accurate and precise geometric correction on the sub-pixel level, resampling and effective false positives elimination. Furthermore, in change detection-based RS techniques it is of high importance that the image information from the raw remotely sensed satellite images should be sufficiently aligned and registered on the sub-pixel level before the correlation processes. However, the more we focus into detecting geographic entities and its changes on sub-pixel level, more challenges are confronted related to preservation of sub-pixel information during resampling (Inglada et al., 2007; Keren, 1988; Kim et al., 1990; Yamaguchi et al., 2003), correct ortho-rectification and co-registration (Bryant et al., 2003; Saba et al., 2017; Townshend et al., 1992).

To address these issues for correct co-seismic landslides mapping a new change-detection based technique of COSI-Corr has been successfully developed and adopted in the Haiti area after the 2010 earthquake(Saba et al., 2017). Although, COSI-Corr performed well in term of co-seismic landslides detecting in Haiti while using an ideal very high-resolution worldview-2 dataset. The main challenge was to test its transferability and robustness in a rough topographic area of Muzaffarabad for co-seismic landslides detection using a medium resolution ASTER dataset. Owing to COSI-Corr high sensitivity for detecting changes on the sub-pixel level, it is considered vulnerable to detecting many changes caused by vegetation, erosion and variation in a built-up area as false positive values (Saba et al., 2017). Therefore, this study focuses on the influence of various factors like vegetation, sedimentation, erosion and built-up areas on landslides automatic detection accuracy through COSI-Corr, while using medium resolution data has been investigated.

2. Study area

The study area, Muzaffarabad is located in the north of Pakistan. This region is recognized for its dynamic seismic-tectonic activities (Kazmi and Jan, 1997; Zaré et al., 2009). It is tectonically an active part of the Lesser and Sub-Himalayan belt that is located in the core and limbs of the Hazara-Kashmir Syntaxis (Bossart et al., 1988; Calkins et al., 1975) and at the junction of the northwest Himalayas of northern Pakistan (Fig. 1). Therefore, structure plays a key role in the preparation of landslides in the selected study area (Kaneda et al., 2008). An active tectonic Balakot-Bagh Faultline passes through the middle of the Muzaffarabad area (Kazmi and Jan, 1997). Topographically majority of the study area is mountainous and surrounded by steep slopes (Saba et al., 2010). Geology of the study area is comprising of various formations composed of sandstone, limestone, shale, alluvium and siltstone. Colluvium and alluvium deposits are sited at the slopes bottom and drainage lines. A major earthquake with moment magnitude Mw = 7.6 hit the study area in 2005, prompting a seventy-kilometer long rupture along Balakot-Bagh Faultline (Avouac et al., 2006; Kaneda et al., 2008). The 2005 earthquake not only triggered hundreds of landslides but it also destabilized the surrounding slopes (Jayangondaperumal and Thakur, 2008; Saba et al., 2010) by creating fissures, crack and crumbling rubble along the Faultline.

Local geological structures have great influence in shaping local drainage pattern in the area (Kamp et al., 2008). Drainage density and slopes closeness to drainage structures is also associated to the erosional activity at slope bottoms in valleys consequently making areas destabilized that causes slope failures (Gokceoglu and Aksoy, 1996; Jayangondaperumal and Thakur, 2008; Yalcin, 2008).

3. Input data and processing

The methodology process is systematized into two groups of tasks. The first group of tasks (section 3.2 and 3.3) includes ortho-rectification, co-registration and correlation of optical ASTER imagery, with the software, COSI-Corr explained by Leprince et al., (2008) and Saba et al., (2017). The second group of tasks (section 3.4) comprises noise removal or data masking and evaluating the role of various factors causing noise in the results.

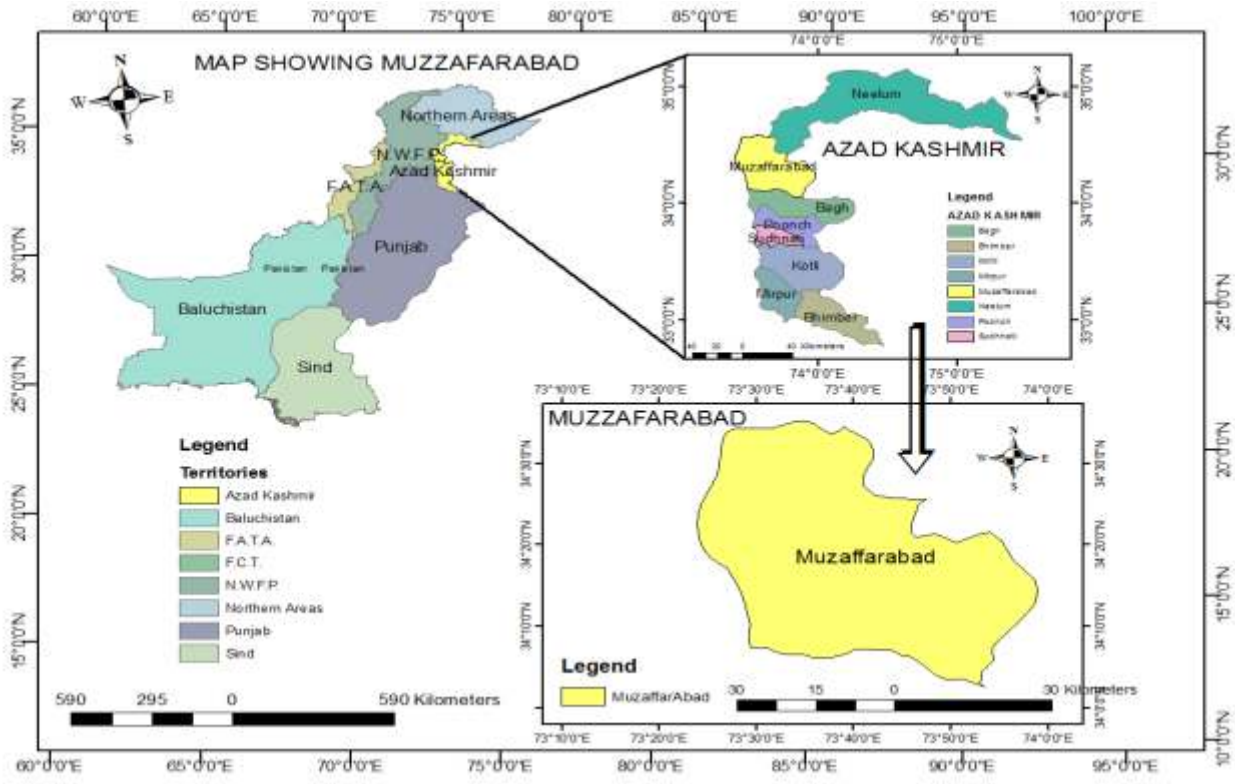

Fig. 1. The relative and absolute location of the study area map.

3.1. Imagery and Digital Elevation Model (DEM)

In this study we used pre- and post-event ASTER level 1A imagery (Table.4.1) with a time span of four years, obtained for November 14, 2001, and October 27, 2005. These images were cloud-free ASTER scenes. Additional pre-and post-event IKONOS and Quickbird images were used for ground control points (GCPs) collection and validation dataset preparation (Saba et al., 2010). The method of automated stereo correlation (Hirano et al., 2003) was used to produce 15 m resolution DEM with the maximum possible level of detail (Table.1). The gaps were filled by the interpolation process. DEM accuracy was checked against GPS points. Drainage pattern was extracted, which were later on used for further analysis while distinguishing landslides from the other displacement values.

3.2. Ortho-rectification/Resampling

For the ortho-rectification of pre-earthquake raw ASTER L1A VNIR image, 20 well spread tie points, located on stable features, away from the deformation zone and image corners were selected from an already ortho-rectified IKONOS imagery. The selected tie points were optimized by using optimization function with five iterations in COSI-Corr, to confirm accurate co-registration between IKONOS and ASTER images. The list of tie points was then converted to GCPs. The GCPs with high residual error were eradicated. The pre-earthquake image was then ortho-rectified and resampled with the calculated GCPs and pre-earthquake DEM. The same procedure was followed for the ortho-rectification of post-event image except for this time the rational polynomial coefficients (RPCs) were selected from the pre-event imagery. According to Leprince et al. , the ideal resampling method sine cardinal (Sinc) was followed for the resampling of both images. The images were then co-registered with a 1/50 of pixel accuracy using Cosi-Corr software , which mean the minimum achievable accuracy for displacement measurement was 1/20 of a pixel (75cm for ASTER 15m). To assume the topography unchanged (as the technique undertakes the unchanged topography throughout the process) before and after the landslide occurrence both the images were ortho-rectified with only the pre-event ASTER DEM.

3.3. Sub-pixel correlation of ASTER optical images

The images were orthorectified, co-registered and aligned to their on-ground seeing geometry. Relative offset values were calculated among both pre- and post-earthquake satellite images. In this method, the correlation is done in dualistic phases. First, it is performed on the supera-pixel scale in which the change among the satellite pre- and post-event images from their associating matrix is extracted taken out. In the second phase, the extracted shift for each pixel is adapted by rounding up the slope variance of both the images by Fourier conversion (Ayoub et al., 2009). The initial window size was set to 32 and the final window size to 4. The step size was kept below the initial window size (at 2). To eliminate any possible outliers, the masking threshold (signal to noise ratio) was kept constant at 0.90. The final correlation was assessed by measuring horizontal shift components that happened in all four directions of east, west, north and south. To evaluate the accuracy of outcomes, a separate layer of the signal to noise ratio was also automatically computed with the correlation, as defined in Leprience et al. (2007). As in this study, we were interested into full displacement of each pixel irrespective of any special direction (east, west, north or south), therefore vectors were calculated by combining the displacement in all four aspect directions.

3.4. Isolation of co-seismic landslide by excluding the following masks

After the application of Cosi-Corr, developed and modified for landslide identification by Saba et al, (2017), the systematic masking was performed to eliminate the high displacement values caused by manmade (construction etc.) and natural activities (erosion, sediment deposition on both sides of streams, deformation due to seismic effects etc.). These masks include drainage lines mask, plane area mask (i.e., very gentle slopes and flat terrain) and NDVI mask (separating vegetated and non-vegetated areas).

3.4.1.Preparation and execution of drainage mask

The high density of false positive values was observed along the banks of rivers and streamlines. Problems due to false positive values in these cases were addressed by subtracting the main drainage lines from the correlation image. The mask was generated by manual digitization of main drainage lines from IKONOS image.

Table 1. Presents spatial and temporal characteristics of the data used in this study, along with details on the acquisition parameters.

Data	Data type	Spatial Resolution	Spectral Res	Acquisition date
ASTER_2000 .hdf	Image (level1A)	15m	Band 3N (Near infrared) 0.78-0.86	14/11/2000
ASTER_2005 .hdf	Image (level1A)	15m	Band 3N (Near infrared) 0.78-0.86	27/10/2005
ASTER_2000	DEM	15m	-	14/11/2000
ASTER_2005	DEM	15m	-	14/11/2000
Landslide inventory	Geo tiff	1m	Created from pan-sharp Ikonos	12/10/2005

3.4.2.Plane area mask construction

As a slope failure is referred as the alteration of a mass of rock, earth or debris down a slope (Cruden, 1991), therefore, the main distinguishing characteristic of false positives values caused by any other feature rather than landslide from the true positives was their presence on plane areas. A mask of the plane and the non-plane area was generated from the ASTER DEM by using internal relief variation filters in ILWIS software (Nijmeijer et al., 2001). If the internal relief of the adjacent pixels was less than 10m within 5*5-pixel window (75m*75m area) then it was classified as plane otherwise un-plane area.

3.4.3.Preparation and execution of vegetation by NDVI mask

In the present study post-event, NDVI was used as a mask of vegetation and non-vegetation areas to eliminate vegetation change effects. Typically, vegetation has NDVI values in the range from 0.1 to 0.7 (Roettger, 2007). Therefore, the threshold of NDVI greater than 0.1 was applied to separate vegetated from non-vegetated areas. The accuracy of the threshold was also tested by overlaying the binary image on the IKONOS imagery of the area available for the same date.

3.5. Accuracy improvement and quality assessment

To assess the quality of measurements after image classification and the application of each mask, accuracy assessment was done for each threshold level (fourteen threshold values) of the map. It was implemented in the form of standard error matrices that compares image classification result with ground truth data (Congalton, 1991; Czaplewski and Catts, 1992; van Oort, 2007).

To further evaluate the results and validity of classification the following derivatives from the error matrix were calculated.

Producer's accuracy was calculated by using a number of correctly classified pixels (e.g. landslides) to the total number of pixels assigned to that category by the ground truth data. It is a measure of error of omission, that occurred when pixels should have been incorporated into the category of "landslide", but were included into "no landslide" category by the classification. In other words, the pixels were omitted from the particular class.

User's accuracy was measured by using the number of correctly classified pixels to the overall number of pixels allocated to a specific category by the classification map. It is a measure of the commission error. Commission error occurred when pixels other than landslides were incorporated into category "landslides" or simply; the pixels were assigned to the wrong class (Jensen, 2005).

The overall accuracy was determined by summing all the correctly identified pixels and dividing it by the sum of all incorrect observation (Jensen, 2005).

Sensitivity is the fraction of positive pixels correctly predicted and "1-specificity" representing the probabilities of committing or an error of commission (false positive).

Specificity is the fraction of negative pixels correctly predicted and "1-sensitivity" represent the probabilities of committing an error of omission (false negative) (i.e., the probability that a pixel not belonging to a particular category is correctly identified.

The receiver operating characteristic curve (ROC curve) plots the rate of true positive to positive classifications against the rate of false positive to negative classifications.

4. Results and discussion

The results were classified into the slide and no-slide classes using various threshold values, as all image algebra change detection algorithms need a suitable threshold selection to identify landslides. The position of the threshold can greatly affect the final accuracy (Fung and LeDrew, 1988). Therefore, we calculated accuracies for 14 different thresholds (displacement value ≥ threshold ="change"), starting from the minimum displacement value to the maximum (Fig. 2). To have a better understanding of the relationship

among the producer's accuracy, user's accuracy, the error of omission and error of commission for each threshold level of the results, we plotted all these values against each other on the same plot (Fig. 2). This also demonstrates the relationship between the threshold variation and its effect on the variation of prediction accuracies. At threshold zero almost all occurred changes were classified as "landslides" and all those points which did not change were classified as "no landslides". The threshold value (0.1) had a large disparity between producer's (97%) and user's (11%) accuracy. This means that 97 percent of landslides are correctly identified but only 11% of the area that is classified as "landslides" is truly landslide.

Producer's accuracy is affected by errors of omission and it reflects the reference field's omission. Conversely, user's accuracy is influenced by errors of commission and it reflects when classified samples are wrongly included.

It is also visible that the error of Omission is low for the first three thresholds (< 20%) but the error of Commission is greater than 80%. This indicates the presence of high confusion which has been caused by a large number of false positives and false negatives present in the results. It also represents that during the time period 2001 to 2005, many pixels were shifted causing high noise even though these pixels were not landslides. In practice, for reducing noise, caused by attitude (roll, pitch, and yaw) artefacts undulating observing platform, the correlation results are de-striped (Ayoub et al., 2008; Necsoiu et al., 2009; Scherler et al., 2008; Teshima and Iwasaki, 2008). However, in this case study, de-striping was actually reducing the accuracy of landslide detection. This indicated that false positives were not produced due to positional errors or platform undulations. Regardless of the fact that both the pre- and post-event image acquisition dates were selected from the same season (October and November) to minimize spectral differences, between the two images; other changes (mostly temporal) i.e. phenology, cloud cover, sun angle and shading directly or indirectly), introduced high complexity in differentiating landslides from other changed features (Jensen, 2005).

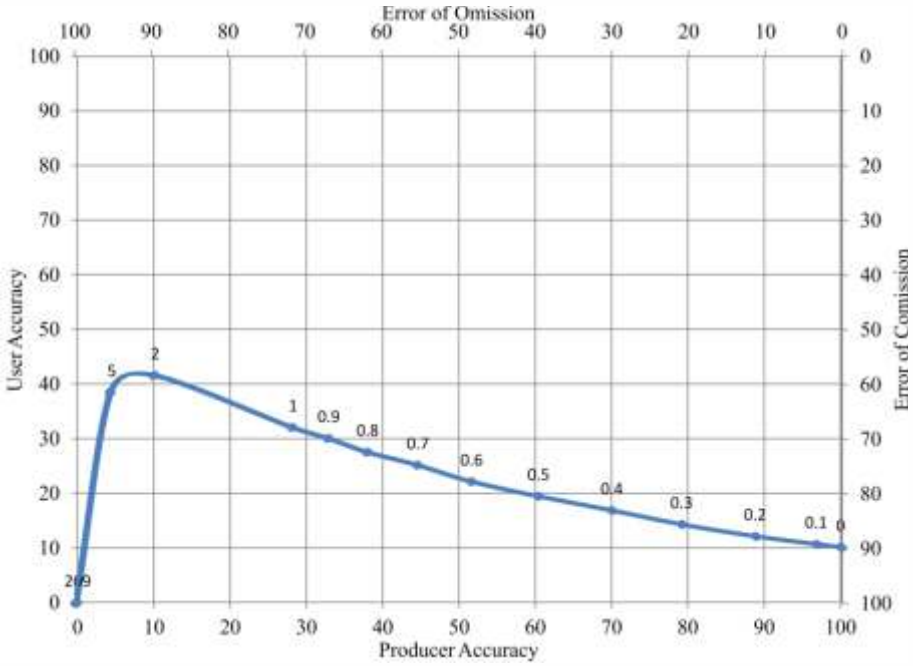

Fig. 2. The curve shows, user accuracy versus producer accuracy on the primary axis and error of omission versus error of commission on a secondary axis for fourteen different threshold values.

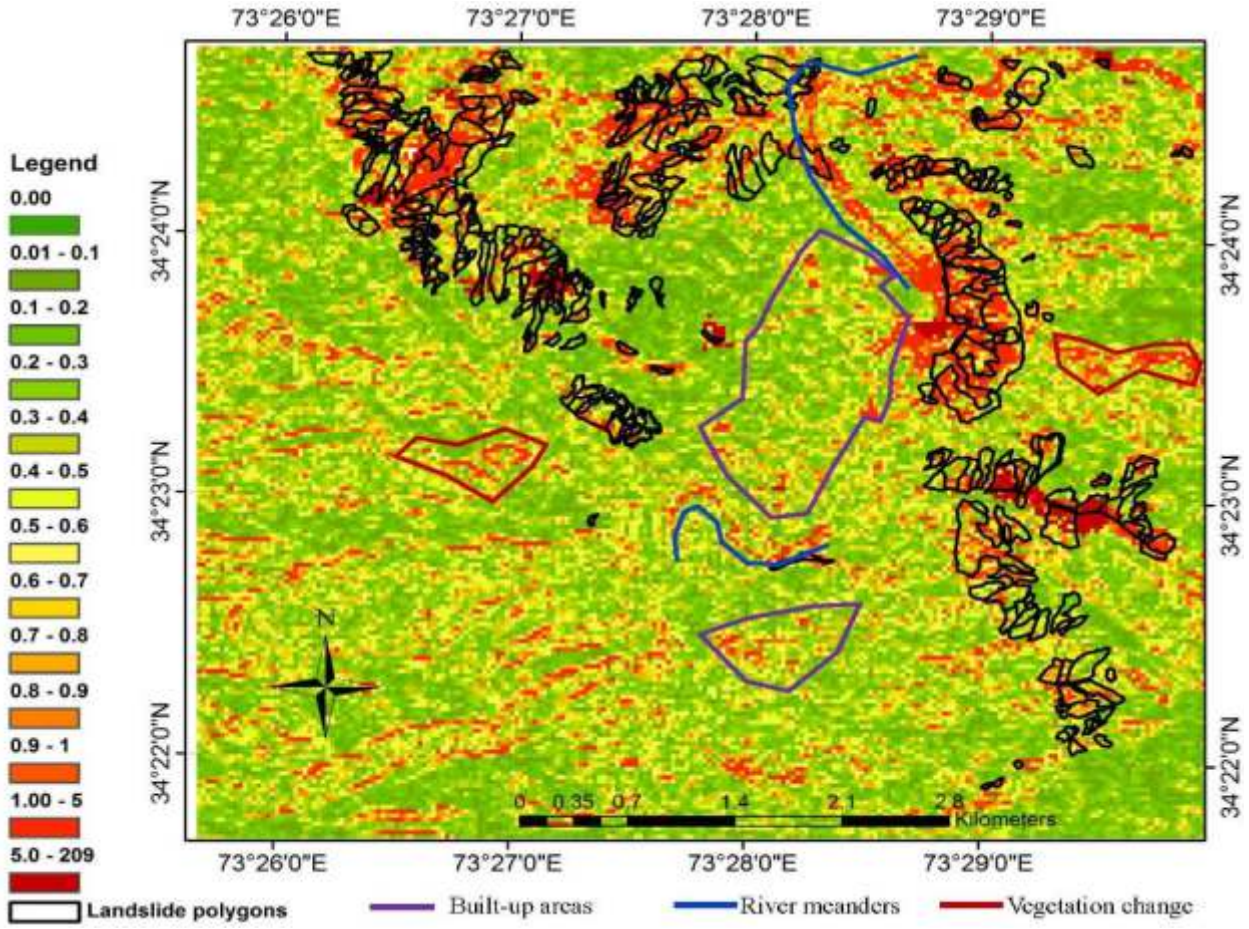

Fig. 3. It shows the correlation results with many noisy patches (changes other than landslides) caused by new constructions, vegetation changes, and river banks erosion and deposition. The details of landslide inventory for this area can be found in (Saba et al., 2010).

In order to distinguish displacements caused due to landslides and other changes, it will be good to select displacement threshold with high producer accuracy and develop rule-set or series of masks for characterizing landslides; and then implement them on the correlation results. To do so, we investigated the false positive showing high displacement values by comparing the high-resolution IKONOS and Quick Bird pre- and post-event images. From the interpretation, it was identified that factors like vegetation change, topographic shadows, erosion, deposition along the drainage lines and urban sprawl were influencing the results. An attempt was made to reduce the number of these false positives by applying a series of different masks. The images were reclassified into binary maps of change (landslide) and no change (no landslide). The accuracy of the reclassified result has been assessed by creating ROC curves. The results have been discussed independently in the following paragraphs after the application of each mask.

4.1. Role of drainage lines

First, the main reason for noise or false positive values in and along the drainage lines (streams, river banks and meanders) were inundation and sedimentation by streams and rivers. This was predominantly visible along the meandering sides of the river Neelum and some narrow stream valleys of Khata Shawai (Fig. 3). Secondly, when approaching towards the landslide toe area along the streamlines, the displacement values are inclined to increase, causing the valley bottom pixels to attain the highest displacement values which are consistent in narrow stream valleys throughout the study area (Fig. 3). The north-south and east-west components of the surface displacement field in these narrow valleys indicated a maximum displacement.

After the introduction of the drainage mask, false positive values have been decreased (Fig. 4). For example, at threshold value 0.1, the false positive rate for landslides has been decreased from 0.93 to 0.87, which is a decrease of 6% error of commission. While for the same threshold, the true positive rate remained almost unchanged with only 0.01 decrease. The decrease in true positive rate is caused by the removal of valleys bottoms along the streamlines, which also eliminated a few pixels that were parts of depositional bodies of landslides. The same increase and decrease trend can be noticed for other threshold values as well (Fig. 4). Generally, the true positive rate for each threshold increased following the drainage mask application.

4.2. Plane area mask

Some false positives were identified in the correlation images due to several natural and man-made changes in urban areas (i.e., new built-up areas, roads pavements, erosion, terracing ground deformation and subsidence, etc.) either located on very gentle slopes or flat terrain. These were eliminated by masking the plane areas (Fig. 5) from the results. After the application of the plane area mask to the correlation results the true positive rate (sensitivity) at threshold value 0.1 remained the same but false positive rate decreased from 0.85 to 0.74, a total of 0.11 (11%) decreases. Elimination of newly constructed buildings on slope areas of southern Muzaffarabad in this period (2001 to 2005) is still difficult to be masked completely with the use of plan area mask. This mask could be further improved by creating a built-up area mask and plane area mask separately.

4.3. Role of vegetation change

Spatial and temporal changes in vegetation over time create significant variation, therefore those areas where vegetation changes had occurred were detected as changed patches and ultimately as landslides. In the past, NDVI has been effectively adopted to differentiate landslides from other changes (Barlow et al., 2006; Schneevoigt et al., 2008). Therefore, in this study, an effort has been made to solve the problem of false positives caused by vegetation changes by masking the areas with vegetation or eliminating areas having NDVI value greater than 0.1.

After the application of the NDVI masks, false positive rate (1-specificity) greatly decreased from 0.74 to 0.9 (Fig. 4). However, at the same time sensitivity also decreased from 0.96 to 0.89.4 (89 %). Now for threshold 0.1, the sensitivity was 0.89, corresponding to only 10.6% probability of an omission error. According to Mather (2004), NDVI also compensates for topography induced variation in scene brightness, which is one of the main reasons for the great decrease of false positive rate (1-specificity). Therefore, it reduced the false positive values caused by vegetation variation due to topographic shadowing differences as well. At the same time, many landslides located in steep slopes shadows were also eliminated causing the decrease in the sensitivity of the map and increase in the error of commission. Another reason which caused the decrease in sensitivity is that even after the failure of slopes, few landslide bodies were intact and were having traces of vegetation. By applying the NDVI mask (areas having NDVI value >0.1), we also deleted those areas which were actually vegetated landslides. Even then the improvement in the elimination of false positives was so high that 1-specificity or false positive rate has decreased from 0.74 to 0.9 (Fig. 4).

Overall by plotting the ROC curve after the application of each mask with respect to all threshold levels, we can see a continuous improvement in the results (Fig. 4). These curves are getting higher after the application of each mask which shows the model is performing better regardless of what threshold is used. Comparison of ROC curves also illustrates that the false positive rate has decreased after the application of each mask; nevertheless, the highest decrease was witnessed after the application of NDVI mask. This indicates that the highest source of commission error was from forest or vegetation change in the study area. Selecting a suitable threshold to separate landslide from no landslide requires a compromise between sensitivity and specificity, as both cannot be maximized concurrently. Therefore, after the application of NDVI mask, if we want to select

an optimal threshold, it will be 0.1 for which both the error of omission and error of commission are reduced to less than 18% (Fig. 4).

The classification results for the selected threshold 0.1, eliminated most of the noise caused by vegetation changes, shadow effects, sedimentation, and erosion along the streamlines, river banks and built-up areas (Fig. 6). Despite the fact that the landslide identification through sub-pixel correlation method results in the noisy performance by showing many changes caused by other factors, it has still performed better than the previous landslide identification techniques.

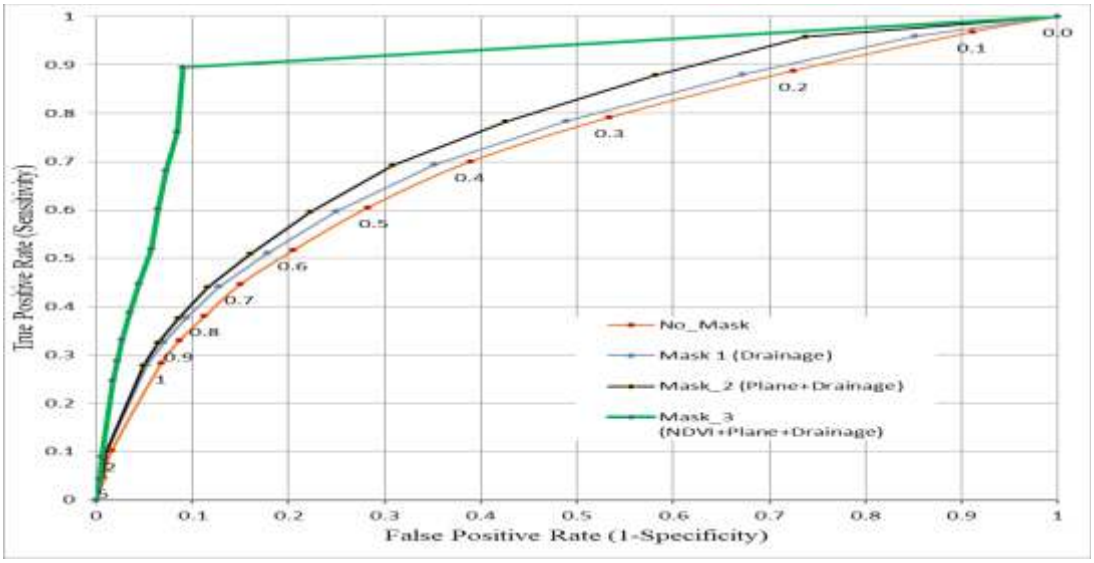

Fig. 4. Relative Operating Characteristic (ROC) curves show the rate of true positives versus false positives for the pure correlation results (no mask) and after the application of each mask, respectively for all the fourteen scenarios or threshold values. All of the curves achieved an increase in the area under the ROC curve after the application of each mask.

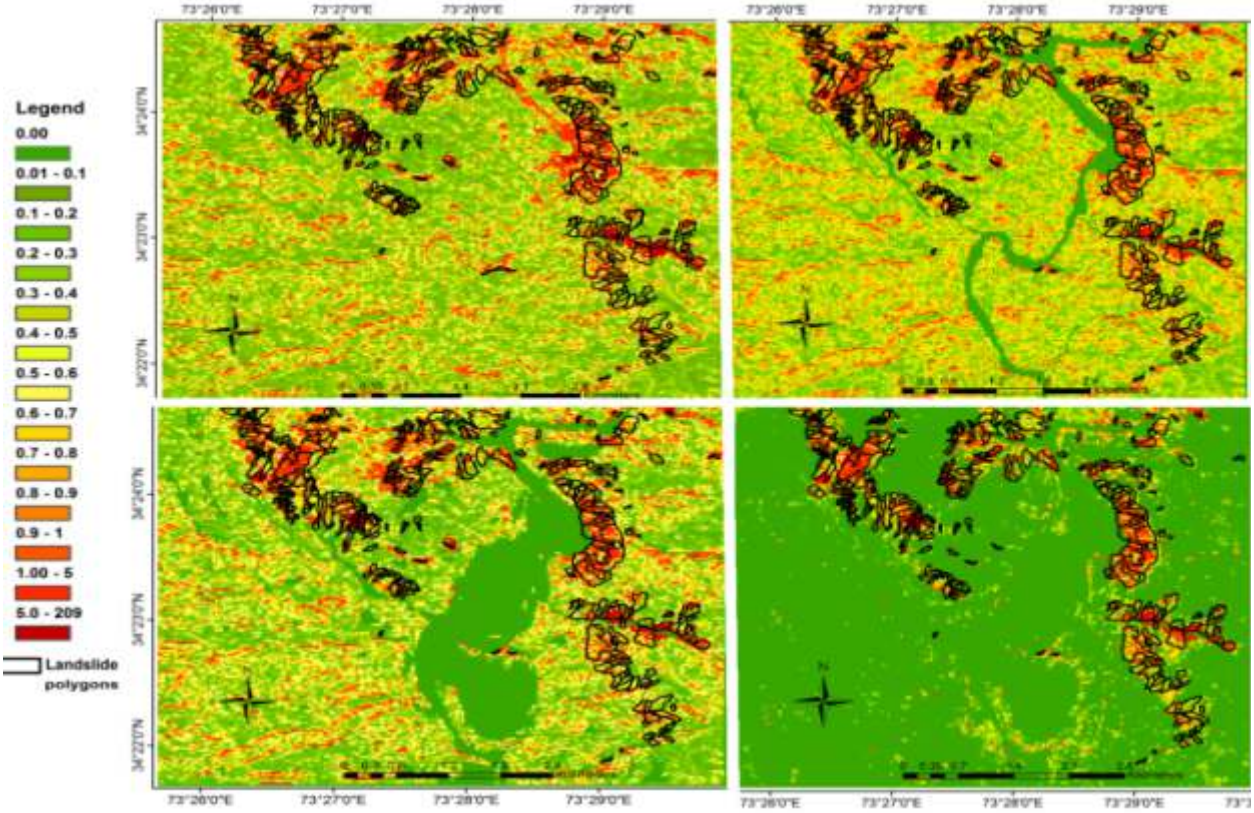

Fig. 5. Top-left shows the correlation results before any mask was applied. The remaining three show the results after the application of each mask, drainage, plain and NDVI, respectively.

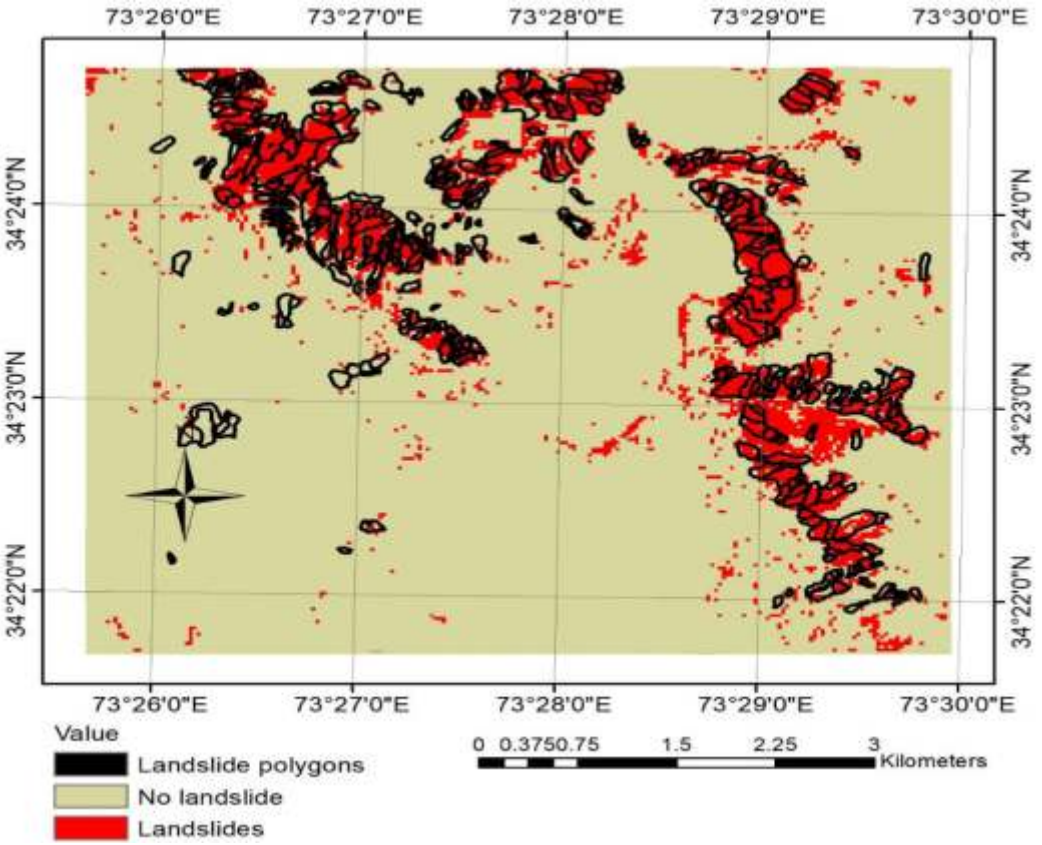

Fig. 6. Shows the classification results for threshold 0.1, overlaid by landslide polygons (ground truth data).

5. Conclusion

This study presents a systematic approach by using a stepwise binary masking idea to enable a significant reduction in false positive from the correlation images, caused by several spatial and temporal changes.

Although this technique for the automatic detection of the landslide on sub-pixel level proves to be one of the best techniques, even then it suffers from some minor problems of having a high number of false positive values. The noise is produced by numerous factors like platform changing attitude through the scanning process, DEM errors, natural features (vegetation change, shadowing effects, erosion and sedimentation) and man-made structures (urbanization). These false positive values degrade the interpretability of the data and decrease the accuracy of the results. Numerous methods have been suggested to deal with the noise produced due to spatial errors (that affect spatial accuracy) like platform attitude problems (Ayoub et al., 2008; Necsoiu et al., 2009; Scherler et al., 2008; Teshima and Iwasaki, 2008), DEM errors (Ayoub et al., 2009; Scherler et al., 2008) and inaccurate resampling and correlation but nothing has been applied to remove the false positive values or thematic errors caused by pixel-shifts representing manmade and natural changes like urban sprawl, spatial and temporal vegetation changes, changes in non-perennial streams and inundation and sedimentation changes in the bi-temporal images.

Hence, landslide automatic identification based on the displacement measurement technique from the bi-temporal imagery alone may not be adequate to detect landslides effectively. Therefore, a detection approach that incorporates data from other sources might be more effective than the one based solely upon the displacement measurement from bi-temporal remote sensing images. This study aimed to investigate the influence of each factor (i.e., vegetation, sedimentation, erosion and built-up areas) contributing to false positives values and an effort has been made to reduce the number of these false positives by combining information from the normalized difference

vegetation index (NDVI), drainage pattern and built-up areas.

The stepwise masking was performed after the application of Cosi-Corr technique (co-registration of optically sensed images and correlation), developed and modified for landslide identification by Saba et al, (2017). The false positives are sequentially eliminated from the landslide class by removing the noises resulting from drainage, urban sprawl and vegetation phonology. The false positives are successively removed from the landslide class by eliminating the noises resulting from drainage, urban sprawl and vegetation phonology. The results accuracy was increased after the application of each mask. The number of false positives were greatly reduced by the application of the vegetation-based mask. The best threshold found was 0.1 for which error of omission and error of commission was less than 11%. The results also showed that medium spatial resolution imagery (ASTER) may well be utilized in an irregular topographic area like the Himalayas to inevitably distinguish above 90% of slope failures. The application of this technique along with considerately prepared masks will additionally enhance the rapid detection of co-seismic landslides on a regional scale in a cost-effective way. Cosi-Corr will also help in evading remote sensing-based techniques that require intensive analysis involving enormous rule-sets. Unlike OBIA technique, that performs well only using high-resolution satellite images (Mondini et al., 2011), Cosi-Corr is claimed to perform well while utilizing medium spatial resolution (5-15m) satellite data Saba et al., (2017). Which makes it economical and possible to be adopted on a regional scale.

Authors contribution

Sumbal Bahar Saba did analysis and writing. Nimat Ullah Khattak did text review. Muhammad Ali did analysis review. Muhammad Waseem statistical analysis and text review. Samina Siddiqui did figures and tables finalization. Seema Anjum did analysis review. Syed Ali Turab did final review of the manuscript.

References

Aghighi, H., Trinder, J., Lim, S., Tarabalka, Y., 2015. Fully spatially adaptive smoothing parameter estimation for Markov random field super-resolution mapping of remotely sensed images. International Journal of Remote Sensing, 36, (11), 2851-2879.

Avouac, J.P., Ayoub, F., Leprince, S., Konca, O., Helmberger, D. V., 2006. The 2005, Mw 7.6 Kashmir earthquake: Sub-pixel correlation of ASTER images and seismic waveforms analysis. Earth and Planetary Science Letters, 249, (3-4), 514-528.

Ayoub, F., Leprince, S., Avouac, J.P., 2009. Co-registration and correlation of aerial photographs for ground deformation measurements. ISPRS Journal of Photogrammetry and Remote Sensing, 64, (6), 551-560.

Ayoub, F., Leprince, S., Binet, R., Lewis, K. W., Aharonson, O., Avouac, J. P., 2008. In Influence of camera distortions on satellite image registration and change detection applications, Geoscience and Remote Sensing Symposium, 2008. IGARSS 2008, IEEE International, II-1072-II-1075.

Barlow, J., Franklin, S., Martin, Y., 2006. High spatial resolution satellite imagery, DEM derivatives, and image segmentation for the detection of mass wasting processes. Photogrammetric Engineering & Remote Sensing, 72, (6), 687-692.

Bossart, P., Dietrich, D., Greco, A., Ottiger, R. Ramsay, J. G., 1988. The tectonic structure of the Hazara-Kashmir syntaxis, southern Himalayas, Pakistan. Tectonics, 7, (2), 273-297.

Bryant, N. Zobrist, A. Logan, T., 2003. In Automatic co-registration of space-based sensors for precision change detection and analysis, Geoscience and Remote Sensing Symposium, 2003. IGARSS '03. Proceedings. 2003 IEEE International, 1372, 1371-1373.

Calkins, J. A., Offield, T. W., Abdullah, S. K., Ali, S. T., 1975. Geology of the southern Himalaya in Hazara, Pakistan, and adjacent areas, 716C.

Casagli, N., Cigna, F., Bianchini, S., Hölbling, D., Füreder, P., Righini, G., Del Conte, S., Friedl, B., Schneiderbauer, S., Iasio, C., Vlcko, J., Greif, V., Proske, H., Granica,

K., Falco, S., Lozzi, S., Mora, O., Arnaud, A., Novali, F., Bianchi, M., 2016. Landslide mapping and monitoring by using radar and optical remote sensing: Examples from the EC-FP7 project SAFER. Remote Sensing Applications: Society and Environment, 4, 92-108.

Congalton, R. G., 1991. A review of assessing the accuracy of classifications of remotely sensed data. Remote Sensing of Environment, 37, (1), 35-46.

Cruden, D. M., 1991. A simple definition of a landslide. Bulletin of the International Association of Engineering Geology, 43, 27-29.

Czaplewski, R. L., Catts, G. P., 1992. Calibration of remotely sensed proportion or area estimates for misclassification error. Remote Sensing of Environment, , 39, (1), 29-43.

Debella-Gilo, M., Kääb, A., 2011. Sub-pixel precision image matching for measuring surface displacements on mass movements using normalized cross-correlation. Remote Sensing of Environment, In Press, Corrected Proof.

Delacourt, C., Allemand, P., Casson, B., Vadon, H., 2004. Velocity field of the “La Clapière” landslide measured by the correlation of aerial and QuickBird satellite images. Geophys. Res. Lett., 31, (15), L15619.

Feizizadeh, B., Blaschke, T., Tiede, D., Moghaddam, M. H. R., 2017. Evaluating fuzzy operators of an object-based image analysis for detecting landslides and their changes. Geomorphology, 293, 240-254.

Fung, T., LeDrew, E., 1988. The Determination of Optimal Threshold Levels for Change Detection Using Various Accuracy indices. Photogrammetric Engineering and Remote Sensing, 54, 1449-1454.

Gokceoglu, C., Aksoy, H., 1996. Landslide susceptibility mapping of the slopes in the residual soils of the Mengen region (Turkey) by deterministic stability analyses and image processing techniques. Engineering Geology, 44, (1-4), 147-161.

Hirano, A., Welch, R., Lang, H., 2003. Mapping from ASTER stereo image data: DEM validation and accuracy assessment. ISPRS Journal of Photogrammetry and Remote Sensing, 57, (5-6), 356-370.

Inglada, J., Muron, V., Pichard, D., Feuvrier, T., 2007. Analysis of Artifacts in Subpixel Remote Sensing Image Registration. Geoscience and Remote Sensing, IEEE Transactions, 45, (1), 254-264.

Jayangondaperumal, R., Thakur, V. C., 2008. Co-seismic secondary surface fractures on southeastward extension of the rupture zone of the 2005 Kashmir earthquake. Tectonophysics, 446, (1-4), 61-76.

Jensen, J. R., 2005. Introductory digital image processing : a remote sensing perspective: Third edition ed.; Prentice-Hall: Upper Saddle River, 526.

Kamp, U., Growley, B. J., Khattak, G. A., Owen, L. A., 2008. GIS-based landslide susceptibility mapping for the 2005 Kashmir earthquake region. Geomorphology, 101, (4), 631-642.

Kaneda, H., Nakata, T., Tsutsumi, H., Kondo, H., Sugito, N., Awata, Y., Akhtar, S. S., Majid, A., Khattak, W., Awan, A. A., Yeats, R. S., Hussain, A., Ashraf, M., Wesnousky, S. G., Kausar, A. B., 2008. Surface Rupture of the 2005 Kashmir, Pakistan, Earthquake and Its Active Tectonic Implications. Bulletin of the Seismological Society of America, 98, (2), 521-557.

Kazmi, A. H., Jan, M. Q., 1997. Geology and Tectonics of Pakistan. Graphic Publishers, Karachi, 554.

Keren, D. A. P., Shmuel., Brada, R., 1988. Image Sequence Enhancement Using Sub-pixel Displacements. In Proceedings of IEEE Conference on Computer Vision and Pattern Recognition, 742-746.

Keyport, R. N., Oommen, T., Martha, T. R., Sajinkumar, K. S., Gierke, J. S., 2018. A comparative analysis of pixel- and object-based detection of landslides from very high-resolution images. International Journal of Applied Earth Observation and Geoinformation, 64, 1-11.

Kim, S. P., Bose, N. K., Valenzuela, H. M., 1990. Recursive reconstruction of high resolution image from noisy undersampled multiframes. Acoustics, Speech and Signal Processing, IEEE Transactions on, 38, (6), 1013-1027.

Lee, S., Lee, M. J., 2006. Detecting landslide location using KOMPSAT 1 and its application to landslide-susceptibility mapping at the Gangneung area, Korea.

Advances in Space Research, 38, (10), 2261-2271.

Leprince, S., 2008. Monitoring Earth surface dynamics with optical imagery. Thesis, California Institute of Technology, California.

Leprince, S., Barbot, S., Ayoub, F., Avouac, J. P., 2007. Automatic and Precise Orthorectification, Coregistration, and Subpixel Correlation of Satellite Images, Application to Ground Deformation Measurements. Geoscience and Remote Sensing, IEEE Transactions on, 45, (6), 1529-1558.

Ling, F., Xiao, F., Du, Y., Xue, H., Ren, X., 2008. Waterline mapping at the subpixel scale from remote sensing imagery with high-resolution digital elevation models. International Journal of Remote Sensing, 29, (6), 1809-1815.

Martha, T. R., Kerle, N., Jetten, V., van Westen, C. J., Kumar, K. V., 2010. Characterising spectral, spatial and morphometric properties of landslides for semi-automatic detection using object-oriented methods. Geomorphology, 116, (1-2), 24-36.

Martin, Y. E., Franklin, S. E., 2005. Classification of soil- and bedrock-dominated landslides in British Columbia using segmentation of satellite imagery and DEM data. International Journal of Remote Sensing, , 26, (7), 1505-1509.

Mather, P. M., 2004. Computer processing of remotely - sensed images : an introduction: 3rd ed.; Wiley & Sons: Chichester , 352.

Mertens, K., Verbeke, L. P., De Wulf, R. R., 2008. Sub-pixel mapping: A comparison of techniques. Ghent, Belgium, Ghent University.

Mondini, A. C., Guzzetti, F., Reichenbach, P., Rossi, M., Cardinali, M., Ardizzone, F., 2011. Semi-automatic recognition and mapping of rainfall induced shallow landslides using optical satellite images. Remote Sensing of Environment, 115, (7), 1743-1757.

Moosavi, V., Talebi, A., Shirmohammadi, B., 2014. Producing a landslide inventory map using pixel-based and object-oriented approaches optimized by Taguchi method. Geomorphology, 204, 646-656.

Keyport, R., Oommen, T., Martha, T., Sajinkumar, K. S., Gierke, J. A., 2018. comparative analysis of pixel- and object-based detection of landslides from very high-resolution images, 64.

Necsoiu, M., Leprince, S., Hooper, D. M., Dinwiddie, C. L., McGinnis, R. N., Walter, G. R., 2009. Monitoring migration rates of an active subarctic dune field using optical imagery. Remote Sensing of Environment, 113, (11), 2441-2447.

Nichol, J., Wong, M. S., 2005. Satellite remote sensing for detailed landslide inventories using change detection and image fusion. International Journal of Remote Sensing, 26, (9), 1913 - 1926.

Nijmeijer, R. G., de Haas, A., Dost, R. J. J., Budde, P. E., 2001. ILWIS 3.0 Academic : user's guide: ITC, ILWIS: Enschede, 530.

Roettger, S., 2007. NDVI-based vegetation rendering: Acta Press Anaheim: Anaheim, 41-45.

Saba, S. B., Ali, M., van der Meijde, M., van der Werff, H., 2017. Co-seismic landslides automatic detection on regional scale with sub-pixel analysis of multi temporal high resolution optical images: Application to southwest of Port au Prince, Haiti. Journal of Himalayan Earth Sciences, 50, (2), 74-92.

Saba, S. B., Van der Meijde, M., Van der Werff, H., 2010. Spatiotemporal landslide detection for the 2005 Kashmir earthquake region. Geomorphology, 124, (1), 17-25.

Saba, S. B., Van der Meijde, M., van der Werff, H., 2010. Spatiotemporal landslide detection for the 2005 Kashmir earthquake region. Geomorphology, 124, (1-2), 17-25.

Scherler, D., Leprince, S., Strecker, M. R., 2008. Glacier-surface velocities in alpine terrain from optical satellite imagery-Accuracy improvement and quality assessment. Remote Sensing of Environment, 112, (10), 3806-3819.

Schneevoigt, N. J., Van der Linden, S., Thamm, H. P., Schrott, L., 2008. Detecting Alpine landforms from remotely sensed imagery. A pilot study in the Bavarian Alps. Geomorphology, 93, (1-2), 104-119.

Sibaruddin, H. I., Shafri, H. Z. M., Pradhan,

Haron, N. A., 2018. Comparison of pixel-based and object-based image classification techniques in extracting information from UAV imagery data. IOP Conference Series: Earth and Environmental Science, 169, (1), 012098.

Teshima, Y., Iwasaki, A., 2008. Correction of Attitude Fluctuation of Terra Spacecraft Using ASTER/SWIR Imagery With Parallax Observation. Geoscience and Remote Sensing, IEEE Transactions on, 46, (1), 222-227.

Thornton, M. W., Atkinson, P. M., Holland, D. A., 2006. Sub-pixel mapping of rural land cover objects from fine spatial resolution satellite sensor imagery using super-resolution pixel-swapping. International Journal of Remote Sensing, 27, (3), 473-491.

Townshend, J. R. G., Justice, C. O., Gurney, C., McManus, J., 1992. The impact of misregistration on change detection. Geoscience and Remote Sensing, IEEE Transactions on, 30, (5), 1054-1060.

Tsai, F., Hwang, J. H., Chen, L. C., Lin, T. H., 2010. Post-disaster assessment of landslides in southern Taiwan after 2009 Typhoon Morakot using remote sensing and spatial analysis. Nat. Hazards Earth Syst. Sci., 10, (10), 2179-2190.

Van Oort, P. A. J., 2007. Interpreting the change detection error matrix. Remote Sensing of Environment, 108, (1), 1-8.

Vu, T. T., Matsuoka, M., Yamazaki, F., 2005. Detection and animation of damage using very high-resolution satellite data following the 2003 Bam, Iran, Earthquake. Earthquake Spectra, 21, (S1), 319-327.

Weirich, F., Blesius, L., 2007. Comparison of satellite and air photo based landslide susceptibility maps. Geomorphology, 87, (4), 352-364.

Yalcin, A., 2008. GIS-based landslide susceptibility mapping using analytical hierarchy process and bivariate statistics in Ardesen (Turkey): Comparisons of results and confirmations. CATENA, 72, (1), 1-12.

Yamaguchi, Y., Tanaka, S., Odajima, T., Kamai, T., Tsuchida, S., 2003. Detection of a landslide movement as geometric misregistration in image matching of SPOT HRV data of two different dates. International Journal of Remote Sensing, 24, (18), 3523 - 3534.

Zaré, M., Karimi-Paridari, S., MonaLisa., 2009. An investigation on Balakot, Muzaffarabad (Pakistan) earthquake, 8 Oct. 2005, Mw 7.6; geological aspects and intensity distribution. Journal of Seismology, 13, (3), 327-337.